Exponential Stabilization of Fully Actuated Planar Bipedal Robotic Walking With Global Position Tracking Capabilities

Yan Gu
School of Mechanical Engineering,
Purdue University,
West Lafayette, IN 47906
e-mail: gu49@purdue.edu

Bin Yao[1]
Professor
School of Mechanical Engineering,
Purdue University,
West Lafayette, IN 47906;
The State Key Laboratory of Fluid Power
and Mechatronic Systems,
Zhejiang University,
Hangzhou, Zhejiang 310027, China
e-mail: byao@purdue.edu

C. S. George Lee
School of Electrical and Computer Engineering,
Purdue University,
West Lafayette, IN 47906
e-mail: csglee@purdue.edu

This paper focuses on the development of a model-based feedback controller to realize high versatility of fully actuated planar bipedal robotic walking. To conveniently define both symmetric and asymmetric walking patterns, we propose to use the left and the right legs for gait characterization. In addition to walking pattern tracking error, a biped's position tracking error in Cartesian space is included in the output function in order to enable high-level task planning and control such as multi-agent coordination. A feedback controller based on input–output linearization and proportional–derivative control is then synthesized to realize exponential tracking of the desired walking pattern as well as the desired global position trajectory. Sufficient stability conditions of the hybrid time-varying closed-loop system are developed based on the construction of multiple Lyapunov functions. In motion planning, a new method of walking pattern design is introduced, which decouples the planning of global motion and walking pattern. Finally, simulation results on a fully actuated planar biped show the effectiveness of the proposed walking strategy. [DOI: 10.1115/1.4038268]

1 Introduction

There are a variety of approaches to realize bipedal robotic walking. One of the most frequently used methods is based on the zero moment point (ZMP) balance criterion [1,2]. Enforcing the ZMP criterion turns a biped into a fixed-based robot manipulator as it requires flat-footed walking, which results in limited walking speed.

The concept of viability has been introduced to walking control [3,4], and capturability has been proposed as a computationally feasible approximation of viability [5–8]. Because capturability is defined based on the viability of walking instead of the state of balance, the associated walking strategies may be less conservative than the ZMP-based approach.

Another approach to realizing bipedal robotic walking is based on nonlinear control theories and the concept of hybrid zero dynamics (HZD) [9–13]. With the HZD framework, the walking stabilization problem becomes a stabilization problem of the closed-loop control system. Orbitally, asymptotic stabilization of an underactuated walking biped with hybrid dynamics was first achieved based on feedback control under the assumption of finite time convergence during the continuous walking phase [9]. Later on, finite time stabilization was relaxed to sufficiently fast exponential stabilization, and the concepts of virtual constraints and HZD were introduced [12–14]. Because the HZD framework only specifies a general structure of walking dynamics, it can be applied to a variety of biped models. In addition to provable closed-loop stability of the control system, another advantage of the HZD-based approach is the achievable high walking speed. Furthermore, the walking strategy based on HZD has been extended to rough terrain walking [15], three-dimensional walking [16], and neutrally stable walking [17]. Besides the HZD framework, orbital stabilization of underactuated walking has also been realized based on transverse linearization [18–20].

For fully actuated walking, the HZD framework has been extended to achieve exponential tracking of the desired walking pattern as well as the desired walking speed [11,21,22]. However, because orbital stabilization cannot control a biped's global position trajectory in Cartesian space, only velocity tracking has been addressed. Therefore, satisfactory position tracking in Cartesian space is not guaranteed, and the walking versatility is limited. Controlling a biped's global position trajectory is desirable because it enables high-level task planning and control such as multi-agent coordination and obstacle avoidance.

Also, previous studies on orbital stabilization typically utilize the traditional support-swing gait characterization that describes a bipedal gait using the support and the swing legs. This gait characterization can be used to conveniently define symmetric gaits but not asymmetric gaits. Therefore, planning and control of asymmetric bipedal robotic gaits have not been fully investigated in previous studies. However, asymmetric gait tracking is potentially meaningful for related research areas such as motion planning and control of prosthetic devices and exoskeletons because asymmetric gaits are common in injured human walking.

In this study, exponential stabilization of fully actuated planar bipedal walking is realized with enhanced versatility as compared with the previous studies on orbital stabilization. The left–right gait characterization is utilized to describe a bipedal gait so as to conveniently define both symmetric and asymmetric gaits. Although this type of gait characterization has been previously adopted [23], planning and control of asymmetric walking have not been fully studied. Another benefit of the left–right gait characterization is that the states representing joint positions become continuous and well defined upon a swing-foot landing. In control design, input–output linearization is utilized to synthesize a controller to achieve exponential tracking of the desired global motion and walking pattern, and the closed-loop stability conditions are derived based on the construction of multiple Lyapunov functions [24]. In motion planning, a new method of walking pattern design is presented, which not only guarantees that the planned motion respects the impact events but also enables decoupled planning of the desired global position trajectory and the desired walking pattern. The proposed walking strategy is validated through simulated walking of a planar biped model with three revolute joints. Simulation results show that the proposed control design can achieve exponential tracking of the desired global position trajectory in Cartesian space as well as the desired

[1]Corresponding author.

Contributed by the Dynamic Systems Division of ASME for publication in the Journal of Dynamic Systems, Measurement, and Control. Manuscript received February 19, 2017; final manuscript received October 19, 2017; published online December 19, 2017. Assoc. Editor: Hashem Ashrafiuon.

walking pattern in the configuration space. A comparison with previous studies on orbital stabilization is also presented to validate the improved versatility.

In Sec. 2, the left–right gait characterization and the full-order hybrid walking dynamics are presented along with the tracking error of the desired position trajectory in Cartesian space and the desired walking pattern. A model-based feedback control law based on input–output linearization is presented in Sec. 3. In Sec. 4, the closed-loop stability is analyzed based on the construction of multiple Lyapunov functions. A new method of walking pattern design is proposed in Sec. 5, which enables decoupled planning of global motion and walking pattern. In Sec. 6, improved versatility of the proposed walking strategy as compared with previous studies is illustrated through simulations, and the effects of control gains on the closed-loop stability are analyzed.

Preliminary results of control design and stability analysis presented in this paper were initially reported in Ref. [25]. The present paper includes important results of motion planning and fully developed theorems on stability analysis, which were omitted from Ref. [25]. Also, a comparison with previous work on versatility is presented through simulations.

2 Problem Formulation

The objective of this study is to achieve exponentially stable walking with high versatility so that a fully actuated planar bipedal robot can exponentially track the desired walking pattern, both symmetric and asymmetric, as well as the desired global position trajectory in Cartesian space. In order to reach this goal, a bipedal gait is characterized by the left and the right legs instead of the traditional characterization by the support and the swing legs, the full-order hybrid walking dynamics are modeled under the left-right gait characterization, and the expressions of the walking pattern tracking error and the global position tracking error are derived.

2.1 Gait Characterization. The traditional gait characterization describes a bipedal gait using the support and the swing legs [9,20,21]. Under the support-swing gait characterization, the states that represent positions and velocities of the support and the swing legs are always discontinuous at the end of a step because of the role switching of the support and the swing legs. Here, we utilize the left–right gait characterization to describe a bipedal gait. There are two main advantages of using the left and the right legs for gait characterization. First, the states that represent joint positions will be continuous and well defined upon an impact [23,26,27]. Although the states that represent joint velocities may still experience sudden jumps due to landing impacts, the definition of these states is at least consistent. Second, the left–right gait characterization enables planning and control of asymmetric gaits, which will be detailed in Secs. 3 and 5.

With the left–right gait characterization, the full-order walking dynamics are presented in Secs. 2.2–2.4.

2.2 Hybrid Walking Dynamics With Impulse Effects. In this study, a fully actuated planar biped with three revolute joints, identical legs, and massless thin feet is considered (see Fig. 1). There are two actuators at the hip and one at each ankle, and three of them are active at any moment except for the one at the swing ankle. Assume that the swing foot always lands flat and remains in static, full contact with the walking surface until the next landing occurs. Under this assumption, the biped is considered fully actuated during continuous phases because it has three degrees-of-freedom during continuous phases and three independent active actuators. Also, assume that the landing impact is a rigid-body contact with an impulse effect and that the double-support phase is instantaneous [9]. Without loss of generality, suppose that the swing leg length is adjustable. Otherwise, when the swing leg passes the support leg, the planar biped with a compass gait can only avoid scuffing the walking surface exactly at the vertical configuration of both legs [9].

Let $Q \subset \mathbb{R}^3$ be the configuration space of the biped when its support foot is in static, full contact with the walking surface and the joint position limits are satisfied. As shown in Fig. 1, let $\mathbf{q}$ denote the joint position vector of the bipedal robot

$$\mathbf{q} = [q_1, \quad q_2, \quad q_3]^{\mathrm{T}} \in Q \tag{1}$$

where q_1, q_2, and q_3 represent the joint angles of the left leg, the right leg, and the trunk with respect to the world coordinate frame $O_wX_wZ_w$, respectively.

Let $\mathbf{u}$ denote the joint torque vector

$$\mathbf{u} = [u_1, \quad u_2, \quad u_3, \quad u_4]^{\mathrm{T}} \in \mathbb{R}^4 \tag{2}$$

where u_1, u_2, u_3, and u_4 are defined as in Fig. 1.

Based on the left–right gait characterization introduced in Sec. 2.1, a complete walking cycle (or, a stride) consists of two successive steps, which include two single-support phases (SSP) and two swing-foot landings. The two SSPs are the left-in-support SSP and the right-in-support SSP. The two swing-foot landings are the left-to-right-support landing and the right-to-left-support landing. System dynamics during the two SSPs are continuous time, but the swing-foot landings are modeled as impulse effects.

When the swing foot hits the walking surface, a landing impact occurs. This switching event can be defined by a switching surface $S_i(\mathbf{q}, \dot{\mathbf{q}})$ $(i \in \{L, R\})$ as

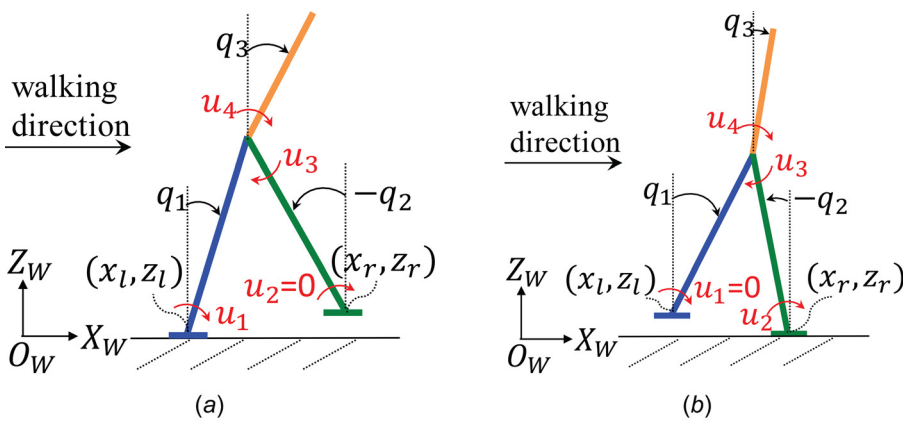

Fig. 1 A bipedal robot walking in the X_w-Z_w plane: (*a*) left leg in support and (*b*) right leg in support

$$\begin{cases} \text{left-to-right-support}: \\ S_L(\mathbf{q},\dot{\mathbf{q}}) := \left\{ (\mathbf{q},\dot{\mathbf{q}}) \in TQ : h_L(\mathbf{q}) = 0, \dfrac{dh_L}{d\mathbf{q}}\dot{\mathbf{q}} < 0 \right\} \\ \text{right-to-left-support}: \\ S_R(\mathbf{q},\dot{\mathbf{q}}) := \left\{ (\mathbf{q},\dot{\mathbf{q}}) \in TQ : h_R(\mathbf{q}) = 0, \dfrac{dh_R}{d\mathbf{q}}\dot{\mathbf{q}} < 0 \right\} \end{cases} \tag{3}$$

where the subscript $i \in \{L, R\}$ indicates whether the left (L) or the right (R) leg is in support, $h_L(\mathbf{q}) := l\cos(q_1) - l\cos(q_2)$ is the swing foot height when the left leg is in support, and $h_R(\mathbf{q}) := l\cos(q_2) - l\cos(q_1)$ is the swing foot height when the right leg is in support (l is the leg length).

Under the assumption that the support foot is in static, full contact with the walking surface, that a double-support phase is instantaneous, and that the landing impact is a rigid-body contact with an infinitesimally small period, the hybrid walking dynamics can be compactly expressed as

$$\begin{cases} \Sigma_L : \begin{cases} \mathbf{M}_L(\mathbf{q})\ddot{\mathbf{q}} + \mathbf{h}_L(\mathbf{q},\dot{\mathbf{q}}) = \mathbf{B}_L\mathbf{u}_L, \text{if}(\mathbf{q}^-,\dot{\mathbf{q}}^-) \notin S_L(\mathbf{q},\dot{\mathbf{q}}) \\ [\mathbf{q}^+;\dot{\mathbf{q}}^+] = \boldsymbol{\Delta}_L(\mathbf{q}^-,\dot{\mathbf{q}}^-), \text{if}(\mathbf{q}^-,\dot{\mathbf{q}}^-) \in S_L(\mathbf{q},\dot{\mathbf{q}}) \end{cases} \\ \Sigma_R : \begin{cases} \mathbf{M}_R(\mathbf{q})\ddot{\mathbf{q}} + \mathbf{h}_R(\mathbf{q},\dot{\mathbf{q}}) = \mathbf{B}_R\mathbf{u}_R, \text{if}(\mathbf{q}^-,\dot{\mathbf{q}}^-) \notin S_R(\mathbf{q},\dot{\mathbf{q}}) \\ [\mathbf{q}^+;\dot{\mathbf{q}}^+] = \boldsymbol{\Delta}_R(\mathbf{q}^-,\dot{\mathbf{q}}^-), \text{if}(\mathbf{q}^-,\dot{\mathbf{q}}^-) \in S_R(\mathbf{q},\dot{\mathbf{q}}) \end{cases} \end{cases} \tag{4}$$

where $\mathbf{M}_i : Q \to \mathbb{R}^{3\times3}$ is the inertia matrix, $\mathbf{h}_i : TQ \to \mathbb{R}^3$ is the sum of the Coriolis, centrifugal, and gravitational terms, $\mathbf{B}_i \in \mathbb{R}^{3\times3}$ is a nonsingular input matrix, $u_i \in \mathbb{R}^3$ is the torque vector of the active joints, and the reset map $\boldsymbol{\Delta}_i : TQ \to \mathbb{R}^6$ represents landing impact dynamics. The expression of $\boldsymbol{\Delta}_i(\mathbf{q},\dot{\mathbf{q}})$ can be obtained as

$$\boldsymbol{\Delta}_i(\mathbf{q},\dot{\mathbf{q}}) := \begin{bmatrix} \mathbf{q} \\ \mathbf{I}_i(\mathbf{q})\dot{\mathbf{q}} \end{bmatrix}, \quad i \in \{L, R\} \tag{5}$$

where the derivation of $\mathbf{I}_i : Q \to \mathbb{R}^{3\times3}$ is given in Ref. [28]. Equation (5) indicates that the states representing joint velocities may experience a sudden jump at the switching event, but the states representing joint positions are always continuous because of the left–right gait characterization.

2.3 Tracking Error of the Desired Global Position Trajectory. To accomplish complex tasks such as multi-agent coordination and obstacle avoidance, it is necessary for a biped to follow the desired travel path with the desired motion in Cartesian space, which can be formulated as a contouring control problem in general. By constructing an orthogonal global task coordinate frame along the desired travel path, the contour error and the motion along the desired travel path can be separately represented in two sets of coordinates, based on which contour error minimization and desired motion following along the contour can be decoupled into a stabilization problem and a trajectory tracking problem [29]. In this study, we want to solve this contouring control problem for the fully actuated planar biped model in Fig. 1, which reduces to the problem of position trajectory tracking along the X_w-axis because the X_w-axis is the only feasible travel path for the planar biped. The complete problem of contouring control will be considered in our future work on three-dimensional walking of fully actuated bipedal robots.

Suppose that the walking direction aligns with the positive direction of the X_w-axis of the world coordinate frame (see Fig. 1). Let (x_l, z_l) and (x_r, z_r) be the left foot and the right foot positions in the world coordinate frame, respectively. Let the biped's hip position s along the X_w-axis represent its global position in Cartesian space. With reference to Fig. 1, s can be expressed as

$$s = \begin{cases} x_l + l\sin(q_1) & \text{(left-in-support)} \\ x_r + l\sin(q_2) & \text{(right-in-support)} \end{cases} \tag{6}$$

Let $s_d(t)$ denote the desired trajectory of s along the X_w-axis. Then, the tracking error of the desired global position trajectory $s_d(t)$ can be expressed as $s - s_d(t)$.

Let

$$q_{\text{st}} := \begin{cases} q_1 & \text{(left-in-support)} \\ q_2 & \text{(right-in-support)} \end{cases}$$

be the support-leg angle. Under the assumption that the support foot position is known, the desired position trajectory of the support leg can be obtained from $s_d(t)$ as

$$q_{\text{std}}(t) := \begin{cases} q_{1d}(t) := \sin^{-1}\left(\dfrac{s_d(t) - x_l}{l}\right) & \text{(left-in-support)} \\ q_{2d}(t) := \sin^{-1}\left(\dfrac{s_d(t) - x_r}{l}\right) & \text{(right-in-support)} \end{cases} \tag{7}$$

Then, the tracking error of $q_{\text{st}} - q_{\text{std}}(t)$ can be used to indicate the global position tracking error $s - s_d(t)$. If a control law is synthesized such that $q_{\text{st}} - q_{\text{std}}(t)$ is driven to zero exponentially, then the exponential tracking of the desired global position trajectory $s_d(t)$ is realized.

2.4 Tracking Error of the Desired Walking Pattern. A walking pattern is defined as the relative evolution of a biped's joint positions with respect to a reference (or, encoding) variable in a complete walking cycle [9]. Tracking a preplanned walking pattern is desirable partly because the joint motion can be synchronized with respect to the reference variable. Furthermore, a proper walking pattern design can be utilized to construct the hybrid invariance of the desired motion, which will be detailed in Sec. 5.

Let

$$\bar{s} = \begin{cases} s - x_l & \text{(left-in-support)} \\ s - x_r & \text{(right-in-support)} \end{cases} \tag{8}$$

be the relative position of the hip with respect to the support foot along the X_w-axis. Note that $\bar{s}(t)$ increases monotonically in t during forward walking.

With $\bar{s}$ chosen as the reference variable, the desired walking pattern is introduced as

$$\mathbf{g}_i(\bar{s}, q_{\text{sw}}, q_3) = \mathbf{0}, i \in \{L, R\}$$

where $q_{\text{sw}} := \begin{cases} q_2 & \text{(left-in-support)} \\ q_1 & \text{(right-in-support)} \end{cases}$ represents the swing leg position and $\mathbf{g}_i(\bar{s}, q_{\text{sw}}, q_3)$ is defined as

$$\begin{cases} \text{left-in-support}: & \mathbf{g}_L(\bar{s}, q_{\text{sw}}, q_3) := \begin{bmatrix} q_2 - \phi_{1L}(\bar{s}) \\ q_3 - \phi_{2L}(\bar{s}) \end{bmatrix} \\ \text{right-in-support}: & \mathbf{g}_R(\bar{s}, q_{\text{sw}}, q_3) := \begin{bmatrix} q_1 - \phi_{1R}(\bar{s}) \\ q_3 - \phi_{2R}(\bar{s}) \end{bmatrix} \end{cases} \tag{9}$$

where the functions $\phi_{ji}(\bar{s})$ ($i \in \{L, R\}$, $j \in \{1, 2\}$) will be determined with a new method of walking pattern design in Sec. 5.

Hence, the tracking error of the desired walking pattern is simply $\mathbf{g}_i(\bar{s}, q_{\text{sw}}, q_3)$. If $\mathbf{g}_i(\bar{s}, q_{\text{sw}}, q_3)$ is exponentially driven to zero with a controller design, then exponential tracking of the desired walking pattern is realized.

Now, we will use an example to illustrate why the left–right gait characterization can be utilized to conveniently define an asymmetric gait. From Eqs. (6) and (8), one has

$$\bar{s} = l \sin(q_{\text{st}}) \tag{10}$$

From Eq. (10), a function of q_{st} is introduced to represent $\phi_{ji}(\bar{s})$ as

$$\tilde{\phi}_{ji}(q_{\text{st}}) := \phi_{ji}(\bar{s}) = \phi_{ji}(l \sin(q_{\text{st}})) \tag{11}$$

for $i \in \{L, R\}$ and $j \in \{1, 2\}$. Thus, under the left–right gait characterization, the desired walking pattern of the swing-leg angle q_{sw} with respect to the support-leg angle q_{st} can be expressed as

$$\begin{cases} \text{left-in-support:} & q_2 - \tilde{\phi}_{1L}(q_1) = 0 \\ \text{right-in-support:} & q_1 - \tilde{\phi}_{1R}(q_2) = 0 \end{cases} \tag{12}$$

Such a walking pattern is illustrated in Fig. 2. From the solid lines in Fig. 2, one can see that an asymmetric gait can be conveniently defined by differentiating the left and the right legs because $\tilde{\phi}_{1L}(q_{\text{st}})$ and $\tilde{\phi}_{1R}(q_{\text{st}})$ can be chosen independently. However, as shown by the dashed line in Fig. 2, the traditional walking characterization based on the support and the swing legs can at most represent a symmetric walking pattern where $\tilde{\phi}_{1L}(q_{\text{st}}) = \tilde{\phi}_{1R}(q_{\text{st}}) = \tilde{\phi}_1(q_{\text{st}})$.

3 Feedback Control Based on Input–Output Linearization

The control objective of this study is to realize exponential tracking of the desired walking pattern in the configuration space as well as the desired position trajectory in Cartesian space. As the first step of our ongoing research, it is assumed that there are no modeling errors or disturbances, and input–output linearization is utilized to synthesize the needed controller to achieve the control objectives. Specifically, the swing leg and the trunk are driven to exponentially converge to the desired walking pattern encoded by the support leg angle, and the support leg is driven to realize exponential tracking of the desired motion in Cartesian space.

With this goal in mind and from Eqs. (7), (9), and (11), the output function is designed as the tracking error of the desired global position in Cartesian space and the desired walking pattern

$$\begin{cases} \text{left-in-support:} & \mathbf{y}_L := \mathbf{q} - \mathbf{q}_{Ld}(t, q_1) \\ \text{right-in-support:} & \mathbf{y}_R := \mathbf{q} - \mathbf{q}_{Rd}(t, q_2) \end{cases} \tag{13}$$

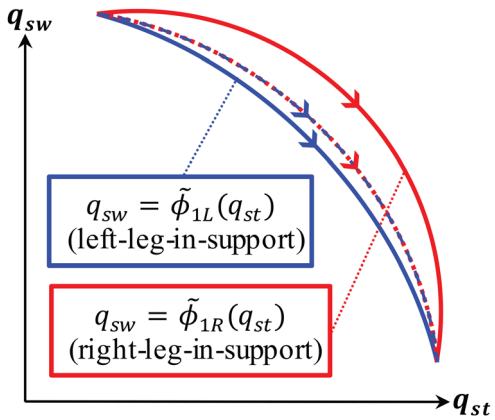

Fig. 2 Encoding the swing-leg pattern using the support-leg angle q_{st} and the swing-leg angle q_{sw}

where

$$\mathbf{q}_{Ld}(t, q_1) := \begin{bmatrix} q_{1d}(t) \\ \tilde{\phi}_{1L}(q_1) \\ \tilde{\phi}_{2L}(q_1) \end{bmatrix} \quad \text{and} \quad \mathbf{q}_{Rd}(t, q_2) := \begin{bmatrix} \tilde{\phi}_{1R}(q_2) \\ q_{2d}(t) \\ \tilde{\phi}_{2R}(q_2) \end{bmatrix}$$

Note that the output function $\mathbf{y}_i$ ($i \in \{L, R\}$) can be designed as three-dimensional because the biped has three independent active actuators. By exponentially driving the output function $\mathbf{y}_i$ ($i \in \{L, R\}$) to zero, exponential tracking of the desired global motion $s_d(t)$ and the desired walking pattern $\mathbf{g}_i(\bar{s}, q_{\text{sw}}, q_3) = \mathbf{0}$ ($i \in \{L, R\}$) can be realized simultaneously.

From Eq. (13), one obtains

$$\ddot{\mathbf{y}}_i = \mathbf{P}_i(q_{\text{st}})\ddot{\mathbf{q}} - \mathbf{z}_i(t, q_{\text{st}}, \dot{q}_{\text{st}}), i \in \{L, R\} \tag{14}$$

during continuous phases, where

$$\mathbf{P}_L := \begin{bmatrix} 1 & 0 & 0 \\ -\dfrac{d\tilde{\phi}_{1L}}{dq_1} & 1 & 0 \\ -\dfrac{d\tilde{\phi}_{2L}}{dq_1} & 0 & 1 \end{bmatrix}, \quad \mathbf{z}_L := \begin{bmatrix} \ddot{q}_{1d}(t) \\ \dfrac{d^2\tilde{\phi}_{1L}}{dq_1^2}\dot{q}_1^2 \\ \dfrac{d^2\tilde{\phi}_{2L}}{dq_1^2}\dot{q}_1^2 \end{bmatrix}$$

$$\mathbf{P}_R := \begin{bmatrix} 1 & -\dfrac{d\tilde{\phi}_{1R}}{dq_2} & 0 \\ 0 & 1 & 0 \\ 0 & -\dfrac{d\tilde{\phi}_{2R}}{dq_2} & 1 \end{bmatrix}, \quad \mathbf{z}_R := \begin{bmatrix} \dfrac{d^2\tilde{\phi}_{1R}}{dq_2^2}\dot{q}_2^2 \\ \ddot{q}_{2d}(t) \\ \dfrac{d^2\tilde{\phi}_{2R}}{dq_2^2}\dot{q}_2^2 \end{bmatrix} \tag{15}$$

From Eq. (15), it can be known that $\mathbf{P}_i(q_{\text{st}})$ is always invertible.

From Eqs. (4) and (14), one has

$$\ddot{\mathbf{y}}_i = \mathbf{N}_i(\mathbf{q})\mathbf{u}_i - \mathbf{L}_i(t, \mathbf{q}, \dot{\mathbf{q}}), \quad i \in \{L, R\} \tag{16}$$

where $\mathbf{N}_i = \mathbf{P}_i\mathbf{M}_i^{-1}\mathbf{B}_i$ is proved to be invertible and $\mathbf{L}_i = \mathbf{P}_i\mathbf{M}_i^{-1}\mathbf{h}_i + \mathbf{z}_i$.

Therefore, the feedback control law based on input–output linearization is defined as

$$\mathbf{u}_i = \mathbf{N}_i^{-1}(\mathbf{v}_i + \mathbf{L}_i) \tag{17}$$

which results in a linear system

$$\ddot{\mathbf{y}}_i = \mathbf{v}_i, \quad i \in \{L, R\} \tag{18}$$

If $\mathbf{v}_i$ is chosen as a proportional–derivative (PD) controller

$$\mathbf{v}_i = -\mathbf{K}_{Pi}\mathbf{y}_i - \mathbf{K}_{Di}\dot{\mathbf{y}}_i, \quad i \in \{L, R\} \tag{19}$$

where $\mathbf{K}_{Pi} \in \mathbb{R}^{3\times3}$ and $\mathbf{K}_{Di} \in \mathbb{R}^{3\times3}$ are both nonsingular diagonal matrices, one then obtains a linear system

$$\dot{\mathbf{x}} = \mathbf{A}_i\mathbf{x}, \quad i \in \{L, R\} \tag{20}$$

with

$$\mathbf{x} := [x_1, x_2, x_3, x_4, x_5, x_6]^{\mathrm{T}} := \begin{bmatrix} \mathbf{y}_i \\ \dot{\mathbf{y}}_i \end{bmatrix} \in \chi \tag{21}$$

and

$$\mathbf{A}_i := \begin{bmatrix} \mathbf{0}_{3\times3} & \mathbf{I}_{3\times3} \\ -\mathbf{K}_{Pi} & -\mathbf{K}_{Di} \end{bmatrix} \in \mathbb{R}^{6\times6} \tag{22}$$

where χ is the full state space, $\mathbf{0}_{3\times3} \in \mathbb{R}^{3\times3}$ is a zero matrix, and $\mathbf{I}_{3\times3} \in \mathbb{R}^{3\times3}$ is an identity matrix.

If $\mathbf{K}_{Pi}$ and $\mathbf{K}_{Di}$ are chosen such that $\mathbf{A}_i$ is Hurwitz, then there exists a real positive-definite-symmetric matrix $\mathbf{W}_i$ such that $V_i(\mathbf{x}) = \mathbf{x}^{\mathrm{T}}\mathbf{W}_i\mathbf{x}$ is a Lyapunov function candidate for the continuous-phase dynamics in Eq. (20) and there exist positive constants c_{1i}, c_{2i}, and c_{3i} ($i \in \{L, R\}$) such that $V_i(\mathbf{x})$ satisfies

$$c_{1i}\|\mathbf{x}\|^2 \le V_i(\mathbf{x}) \le c_{2i}\|\mathbf{x}\|^2 \quad \text{and} \quad \dot{V}_i(\mathbf{x}) \le -c_{3i}V_i(\mathbf{x}) \tag{23}$$

for all $\mathbf{x}$ during continuous phases [30].

4 Stability Analysis

Based on previous analysis, the closed-loop walking dynamics can be compactly written as

$$\begin{cases} \Sigma_L: \begin{cases} \dot{\mathbf{x}} = \mathbf{A}_L\mathbf{x}, & \text{if } (t^-, \mathbf{x}^-) \notin S_{L\to R}(t, \mathbf{x}) \\ \mathbf{x}^+ = \mathbf{\Delta}_{L\to R}(t^-, \mathbf{x}^-), & \text{if } (t^-, \mathbf{x}^-) \in S_{L\to R}(t, \mathbf{x}) \end{cases} \\ \Sigma_R: \begin{cases} \dot{\mathbf{x}} = \mathbf{A}_R\mathbf{x}, & \text{if } (t^-, \mathbf{x}^-) \notin S_{R\to L}(t, \mathbf{x}) \\ \mathbf{x}^+ = \mathbf{\Delta}_{R\to L}(t^-, \mathbf{x}^-), & \text{if } (t^-, \mathbf{x}^-) \in S_{R\to L}(t, \mathbf{x}) \end{cases} \end{cases} \tag{24}$$

where the expressions of $\mathbf{\Delta}_{L\to R}$ and $\mathbf{\Delta}_{R\to L}$ can be derived from $\mathbf{\Delta}_i$ and $\mathbf{y}_i$ and the expressions of the switching surfaces $S_{L\to R}(t, \mathbf{x})$ and $S_{R\to L}(t, \mathbf{x})$ can be obtained from S_i and $\mathbf{y}_i$.

Without loss of generality, suppose that the walking process begins with the left leg in support and the right leg in the air at $t = t_0$. Without loss of generality, suppose $t_0 = 0$. Let T_{L_k} and T_{R_k}, $k \in \{1, 2, \ldots\}$ represent the actual moments of the kth left-to-right-support and the kth right-to-left-support impacts, respectively. Without loss of generality, assume $T_{R_0} = t_0$. Let τ_{L_k} and τ_{R_k}, $k \in \{1, 2, \ldots\}$ denote the desired moments of the kth left-to-right-support impact assuming $\mathbf{x}(t) = 0 \forall t > T_{R_{k-1}}$ and the kth right-to-left-support impact assuming $\mathbf{x}(t) = 0 \forall t > T_{L_k}$, respectively.

Properties of T_{L_k} and T_{R_k} are summarized in Theorem 1, which is introduced based on Lemma 2 in Ref. [31].

THEOREM 1. *Consider the fully actuated walking system in Eq. (24). Let the following conditions hold:*

(A1) There is no beating effect at impacts.
(A2) The desired global position trajectory $s_d(t)$ is continuously differentiable and monotonically increasing for $t > 0$.
(A3) The function $\tilde{\phi}_{ji}(q_{\mathrm{st}})$ ($i \in \{L, R\}$, $j \in \{1, 2\}$) in Eq. (11) is continuously differentiable in q_{st}.

Then, there exists a small neighborhood U of the point $(\tau_{i_k}, 0)$, $i \in \{L, R\}$, $k \in \{1, 2, \ldots\}$ such that $T_{i_k}(\tau_{i_k}, \mathbf{p}_{i_k}(\tau_{i_k}))$ is a unique continuously differentiable function in U, where $\mathbf{p}_{L_k}(t)$ is the solution of $\dot{\mathbf{x}} = \mathbf{A}_L\mathbf{x}$ with initial condition $\mathbf{p}_{L_k}(T^+_{R_{k-1}}) = \mathbf{x}(T^+_{R_{k-1}})$ for $t \in (T_{R_{k-1}}, +\infty)$ and $\mathbf{p}_{R_k}(t)$ is the solution of $\dot{\mathbf{x}} = \mathbf{A}_R\mathbf{x}$ with initial condition $\mathbf{p}_{R_k}(T^+_{L_k}) = \mathbf{x}(T^+_{L_k})$ for $t \in (T_{L_k}, +\infty)$. Also, T_{i_k} has the following properties:

(P1) $T_{L_k}(\tau_{L_k}, \mathbf{0}) = \tau_{L_k}$, $T_{R_k}(\tau_{R_k}, \mathbf{0}) = \tau_{R_k}$; and
(P2) there exists a positive number L_τ such that $|T_{i_k}(\tau, \mathbf{w}) - T_{i_k}(\tau, \mathbf{u})| \le L_\tau\|\mathbf{w} - \mathbf{u}\|$, $\forall(\tau, \mathbf{w})$, $(\tau, \mathbf{u}) \in U$.

Proof. By the definitions of T_{i_k} and τ_{i_k} ($i \in \{L, R\}$, $k \in \{1, 2, \ldots\}$), the property (P1) holds. From the conditions (A1)–(A3) and Eqs. (3), (13), and (24), it can be known that the functions that define the continuous dynamics, the reset maps, and the switching surfaces are all continuously differentiable in t and $\mathbf{x}$. Then, by the implicit function theorem, the property (P2) holds. ■

We are now ready to present the main theorem.

THEOREM 2. Let the conditions (A1)–(A3) hold. Assume that $\mathbf{\Delta}_{L\to R}(\tau^-_{L_k}, \mathbf{0}) = \mathbf{0}$ and $\mathbf{\Delta}_{R\to L}(\tau^-_{R_k}, \mathbf{0}) = \mathbf{0}$ hold for any $k \in \{1, 2, \ldots\}$. Then, there exist positive-definite diagonal matrices $\mathbf{K}_{Pi}$ and $\mathbf{K}_{Di}$ ($i \in \{L, R\}$) and a positive number δ such that the hybrid time-varying closed-loop system in Eq. (24) is locally exponentially stable for all $\mathbf{x}(0) \in B_\delta(\mathbf{0}) := \{\mathbf{x} \in \chi : \|\mathbf{x}\| < \delta\}$.

Proof. Without loss of generality, suppose that the walking process begins with the left-in-support continuous phase.

Let $V_L(\mathbf{x})$ and $V_R(\mathbf{x})$ be the Lyapunov functions associated with the left-in-support and the right-in-support phases, respectively. When the walking process begins with the left-in-support continuous phase, the Kth step ($K \in \{1, 3, 5\ldots\}$) is a left-in-support phase and the Kth switching is a left-to-right-support switching. Let $V_R|^+_K$ and $V_L|^+_{K+1}$ ($K \in \{1, 3, 5, \ldots\}$) denote the values of Lyapunov functions right after the Kth and the $(K+1)$th switchings, respectively. By stability analysis via multiple Lyapunov functions [24], the overall system is exponentially stable if $V_L(\mathbf{x})$ and $V_R(\mathbf{x})$ are exponentially decreasing in the left-in-support and the right-in-support phases, respectively, and if $\{V_R|^+_1, V_R|^+_3, V_R|^+_5 \ldots\}$ and $\{V_L|^+_2, V_L|^+_4, V_L|^+_6 \ldots\}$ are both strictly decreasing sequences.

As explained in Sec. 3, if $\mathbf{K}_{Pi}$ and $\mathbf{K}_{Di}$ ($i \in \{L, R\}$) are chosen such that $\mathbf{A}_i$ is Hurwitz, then the continuous-phase subsystems are exponentially stabilized. Therefore, the remaining task is to derive stability conditions to guarantee that the sequences $\{V_R|^+_1, V_R|^+_3, V_R|^+_5 \ldots\}$ and $\{V_L|^+_2, V_L|^+_4, V_L|^+_6 \ldots\}$ are both strictly decreasing. This requirement can be rewritten as

$$V_R|^+_{K+2} < V_R|^+_K \quad \text{and} \quad V_L|^+_{K+3} < V_L|^+_{K+1} \tag{25}$$

where K is defined as

$$K \in \{1, 3, 5, \ldots\}$$

for the rest of this proof.

First, we prove that there exist positive-definite diagonal matrices $\mathbf{K}_{Pi}$ and $\mathbf{K}_{Di}$ ($i \in \{L, R\}$) and a positive number δ_R such that $V_R|^+_{K+2} < V_R|^+_K$ for any $\mathbf{x}(0) \in B_{\delta_R}(\mathbf{0})$.

From Eq. (23), one has

$$V_R(\mathbf{x}) \le e^{-c_{3R}(t-T_K)}V_R|^+_K \tag{26}$$

during the continuous-phase right after the Kth impact and

$$V_L(\mathbf{x}) \le e^{-c_{3L}(t-T_{K+1})}V_L|^+_{K+1} \tag{27}$$

during the continuous-phase right after the $(K+1)$th impact.

Because of the assumption $\mathbf{\Delta}_{R\to L}(\tau^-_{K+1}, \mathbf{0}) = \mathbf{0}$, one has

$$\begin{aligned} \|\mathbf{x}|^+_{K+1}\| &= \|\mathbf{\Delta}_{R\to L}(T^-_{K+1}, \mathbf{x}|^-_{K+1})\| \\ &\le \|\mathbf{\Delta}_{R\to L}(T^-_{K+1}, \mathbf{x}|^-_{K+1}) - \mathbf{\Delta}_{R\to L}(\tau^-_{K+1}, \mathbf{x}|^-_{K+1})\| \\ &\quad + \|\mathbf{\Delta}_{R\to L}(\tau^-_{K+1}, \mathbf{x}|^-_{K+1}) - \mathbf{\Delta}_{R\to L}(\tau^-_{K+1}, 0)\| \end{aligned} \tag{28}$$

where T_{K+1} is the moment of the actual $(K+1)$th impact, $\mathbf{x}|^-_{K+1}$ and $\mathbf{x}|^+_{K+1}$ represent the values of $\mathbf{x}$ right before and after the $(K+1)$th impact, respectively, and τ_{K+1} is the moment of the desired $(K+1)$th impact assuming $\mathbf{x}(t) = \forall t > T_K$.

Because the reset map $\mathbf{\Delta}_{R\to L}(t, \mathbf{x})$ is continuously differentiable in t and $\mathbf{x}$, it is locally Lipschitz continuous in t and $\mathbf{x}$. Hence, there exists $r^*_R > 0$ such that for any $\mathbf{x}(0) \in B_{r^*_R}(\mathbf{0})$, one has

$$\|\mathbf{\Delta}_{R\to L}(\tau^-_{K+1}, \mathbf{x}|^-_{K+1}) - \mathbf{\Delta}_{R\to L}(\tau^-_{K+1}, \mathbf{0})\| \le L_{\mathbf{\Delta}_{Rx}}\|\mathbf{x}|^-_{K+1}\| \tag{29}$$

and

$$\|\mathbf{\Delta}_{R\to L}(T^-_{K+1}, \mathbf{x}|^-_{K+1}) - \mathbf{\Delta}_{R\to L}(\tau^-_{K+1}, \mathbf{x}|^-_{K+1})\| \le L_{\mathbf{\Delta}_{Rt}}|T_{K+1} - \tau_{K+1}| \tag{30}$$

for some Lipschitz constants $L_{\mathbf{\Delta}_{Rx}}$ and $L_{\mathbf{\Delta}_{Rt}}$.

Define

$$\tilde{\mathbf{x}}_R(t) := e^{\mathbf{A}_R(t-T_K)}\mathbf{x}|^+_K, \quad \forall t > T_K \tag{31}$$

By Theorem 1, there exist $h_R^* > 0$ and $L_\tau > 0$ such that

$$|T_{K+1} - \tau_{K+1}| = |T_{K+1}(\tau_{K+1}, \tilde{\mathbf{x}}(\tau_{K+1})) - T_{K+1}(\tau_{K+1}, \mathbf{0})| \le L_\tau \|\tilde{\mathbf{x}}_R(\tau_{K+1})\| \tag{32}$$

for any $\mathbf{x}(0) \in B_{h_R^*}(\mathbf{0})$.

From Eqs. (28)–(30), and (32), one has

$$\|\mathbf{x}|_{K+1}^+\|^2 \le L_{\Delta_R}(\|\mathbf{x}|_{K+1}^-\|^2 + \|\tilde{\mathbf{x}}_R(\tau_{K+1})\|^2) \tag{33}$$

where $L_{\Delta_R} := \max(2L_{\Delta_{Rx}}^2, 2L_{\Delta_{Rt}}^2 L_\tau^2)$.

Similarly

$$\|\mathbf{x}|_{K+2}^+\|^2 \le L_{\Delta_L}(\|\mathbf{x}|_{K+2}^-\|^2 \|\tilde{\mathbf{x}}_L(\tau_{K+2})\|^2) \tag{34}$$

where L_{Δ_L} is a constant that can be obtained similarly to L_{Δ_R}, and $\tilde{\mathbf{x}}_L(t)$ is defined as

$$\tilde{\mathbf{x}}_L(t) := e^{\mathbf{A}_L(t-T_{K+1})}\mathbf{x}|_{K+1}^+, \quad \forall t > T_{K+1} \tag{35}$$

According to Eq. (23), the following inequalities hold:

$$\begin{aligned} &V_R|_{K+1}^- \ge c_{1R}\|\mathbf{x}|_{K+1}^-\|^2, \quad V_R(\tilde{\mathbf{x}}_R(\tau_{K+1})) \ge c_{1R}\|\tilde{\mathbf{x}}_R(\tau_{K+1})\|^2 \\ &V_L|_{K+2}^- \ge c_{1L}\|\mathbf{x}|_{K+2}^-\|^2, \quad V_L(\tilde{\mathbf{x}}_L(\tau_{K+2})) \ge c_{1L}\|\tilde{\mathbf{x}}_L(\tau_{K+2})\|^2 \\ &V_L|_{K+1}^+ \le c_{2L}\|\mathbf{x}|_{K+1}^+\|^2, \quad V_R|_{K+2}^+ \le c_{2R}\|\mathbf{x}|_{K+2}^+\|^2 \end{aligned} \tag{36}$$

Furthermore, from Eqs. (26), (27), (31), and (35)

$$V_R(\tilde{\mathbf{x}}_R(\tau_{k+1})) \le e^{-c_{3R}(\tau_{k+1}-T_K)}V_R|_K^+ \tag{37}$$

and

$$V_L(\tilde{\mathbf{x}}_L(\tau_{k+2})) \le e^{-c_{3L}(\tau_{k+2}-T_{K+1})}V_L|_{K+1}^+ \tag{38}$$

hold.

Combining Eqs. (32), (34), and (36)–(38), one obtains

$$V_R|_{K+2}^+ \le \frac{c_{2L}c_{2R}}{c_{1R}c_{1L}} L_{\Delta_L} L_{\Delta_R} e^{-(c_{3L}\Delta\tau_{K+1}+c_{3R}\Delta\tau_K)} \times (1 + e^{-c_{3L}(T_{K+2}-\tau_{K+2})})(1 + e^{-c_{3R}(T_{K+1}-\tau_{K+1})})V_R|_K^+ \tag{39}$$

where $\Delta\tau_K := \tau_{K+1} - T_K$ and $\Delta\tau_{K+1} := \tau_{K+2} - T_{K+1}$. Note that $\Delta\tau_K$ is the desired duration of the $(K+1)$th step, which is known right after the Kth actual impact occurs.

From Eqs. (23) and (31),

$$\|\tilde{\mathbf{x}}_R(\tau_{k+1})\| \le \sqrt{\frac{c_{2R}}{c_{1R}}} e^{-\frac{c_{3R}}{2c_{2R}}\Delta\tau_k}\|\mathbf{x}|_K^+\| \tag{40}$$

holds, and thus from Eqs. (32) and (40), one has

$$|T_{K+1} - \tau_{K+1}| \le L_\tau \sqrt{\frac{c_{2R}}{c_{1R}}} e^{-\frac{c_{3R}}{2c_{2R}}\Delta\tau_K}\|\mathbf{x}|_K^+\| \tag{41}$$

Similarly

$$|T_{K+2} - \tau_{K+2}| \le L_\tau \sqrt{\frac{c_{2L}}{c_{1L}}} e^{-\frac{c_{3L}}{2c_{2L}}\Delta\tau_{K+1}}\|\mathbf{x}|_{K+1}^+\| \tag{42}$$

Hence, for any $\varepsilon > 0$, there exist sufficiently large c_{3L} and c_{3R} and a positive number l^* such that

$$e^{-c_{3L}(T_{K+2}-\tau_{K+2})} \le 1 + \varepsilon \quad \text{and} \quad e^{-c_{3R}(T_{K+1}-\tau_{K+1})} \le 1 + \varepsilon \tag{43}$$

hold for all $\mathbf{x}(0) \in B_{l^*}(\mathbf{0})$.

Then, it can be obtained from Eqs. (39) and (43) that

$$V_R|_{K+2}^+ \le \frac{c_{2L}c_{2R}}{c_{1L}c_{1R}} L_{\Delta_L} L_{\Delta_R} (1+\varepsilon)^2 e^{-(c_{3L}\Delta\tau_{K+1}+c_{3R}\Delta\tau_K)}V_R|_K^+ \tag{44}$$

holds for any $\mathbf{x}(0) \in B_{\delta_R}(\mathbf{0})$ where $\delta_R := \min(r_R^*, h_R^*, l^*)$.

Similarly

$$V_L|_{K+3}^+ \le \frac{c_{2L}c_{2R}}{c_{1L}c_{1R}} L_{\Delta_L} L_{\Delta_R} (1+\varepsilon)^2 e^{-(c_{3L}\Delta\tau_{K+3}+c_{3R}\Delta\tau_{K+2})}V_L|_{K+1}^+ \tag{45}$$

holds for any $\mathbf{x}(0) \in B_{\delta_L}(\mathbf{0})$ where δ_L can be obtained similarly to the above analysis.

Note that c_{3i} $(i \in \{L, R\})$ is determined by $\mathbf{K}_{Pi}$ and $\mathbf{K}_{Di}$. Hence, if the PD gains are sufficiently large such that $\mathbf{A}_i$ is Hurwitz and that there exists a positive number $\delta = \min(\delta_L, \delta_R)$ such that

$$c_{3L}\Delta\tau_{K+1} + c_{3R}\Delta\tau_K > 2\ln\left(\frac{c_{2L}c_{2R}}{c_{1L}c_{1R}} L_{\Delta_L} L_{\Delta_R}(1+\varepsilon)\right) \tag{46}$$

and

$$c_{3L}\Delta\tau_{K+3} + c_{3R}\Delta\tau_{K+2} > 2\ln\left(\frac{c_{2L}c_{2R}}{c_{1L}c_{1R}} L_{\Delta_L} L_{\Delta_R}(1+\varepsilon)\right) \tag{47}$$

hold for any $\mathbf{x}(0) \in B_\delta(\mathbf{0})$ and any $K \in \{1, 3, 5,\ldots\}$, then $V_R|_{K+2}^+ < V_R|_K^+$ and $V_L|_{K+3}^+ < V_L|_{K+1}^+$ hold for any $\mathbf{x}(0) \in B_\delta(\mathbf{0})$ and any $K \in \{1, 3, 5,\ldots\}$; i.e., the closed-loop system in Eq. (24) is locally exponentially stable. ■

The stability conditions in Eqs. (46) and (47) indicate that the output function should converge to zero sufficiently fast so as to diminish the possible divergence caused by reset maps. In previous studies, rapidly exponential convergence of output function has been proposed to deal with the possible expansiveness of a landing impact [21], which can also be applied here to further increase the convergence rate.

In Sec. 5, it will be shown that the assumption of $\mathbf{\Delta}_{L\to R}(\tau_K^-, \mathbf{0}) = \mathbf{0}$ and $\mathbf{\Delta}_{R\to L}(\tau_{K+1}^-, \mathbf{0}) = \mathbf{0}$ in Theorem 2 will always hold for any $K \in \{1, 3, 5,\ldots\}$ if the desired walking pattern is designed properly.

5 Desired Walking Pattern Design

The desired walking motion $\mathbf{q}_{id}(t, q_{st})$ $(i \in \{L, R\})$ in Eq. (13) is completely defined by the desired global position trajectory and the desired walking pattern. Suppose that the desired global position trajectory $s_d(t)$ is determined by the high-level task planner, which is continuously differentiable and monotonically increasing for $t > 0$. Then, the remaining task of motion planning is walking pattern design, which should guarantee that the desired motion $\mathbf{q}_{id}(t, q_{st})$ will satisfy the following conditions:

(C1) $\mathbf{\Delta}_{L\to R}(\tau_K^-, \mathbf{0}) = \mathbf{0}$ and $\mathbf{\Delta}_{R\to L}(\tau_{K+1}^-, \mathbf{0}) = \mathbf{0}$, $\forall K \in \{1, 3, 5, \ldots\}$
(C2) forward walking direction;
(C3) ground-contact constraints including the friction cone and the unilateral constraint;
(C4) joint position and velocity limits; and
(C5) joint torque limits.

Since the last four conditions (C2)–(C5), can be easily met through trajectory optimization, they are not further discussed in this paper. The first condition (C1) essentially states that the desired gait should respect the reset map; i.e., if $\mathbf{x}(\tau_K^-) = \mathbf{0}$, then $\mathbf{x}(\tau_K^+) = \mathbf{0}$ should always hold. As presented in Sec. 4, the first condition (C1) is important because it can greatly simplify the stability analysis of the hybrid time-varying closed-loop control system. However, the satisfaction of (C1) is not straightforward as it involves both the desired global position trajectory and the desired walking pattern.

In this section, a new method of walking pattern design is proposed, which guarantees that (C1) is always satisfied for any

feasible $s_d(t)$ that is continuously differentiable and monotonically increasing for $t>0$. This is advantageous because the high-level planning of the desired global position trajectory $s_d(t)$ and the low-level planning of the desired walking pattern represented by $\tilde{\phi}_{ji}(q_{st})$ are decoupled for the satisfaction of (C1).

5.1 Hybrid Invariance of Desired Motion. The condition (C1) can be decomposed into two parts. One part requires that the desired walking pattern should respect the reset map, which can be satisfied based on the same method of walking pattern design for constructing HZD [13]. The other part is tricky to meet, which requires that the desired position trajectory of the support leg should respect the reset map. As indicated in Eq. (7), the desired support-leg trajectory is updated at the beginning of each actual step, and thus it depends on when and where the last actual swing-foot touchdown occurs.

When the walking process begins with the left-in-support continuous phase, the Kth step ($K \in \{1, 3, 5\ldots\}$) is a left-in-support step starting at $t = T^+_{K-1}$, and the Kth desired switching is a left-to-right-support switching at $t = \tau^-_K$. Suppose that the desired walking pattern $\mathbf{g}_L(l\sin(q_1), q_2, q_3) = \mathbf{0}$ has at least one intersection with the switching surface $S_L(\mathbf{q}, \dot{\mathbf{q}})$. Also, suppose that one of these intersections has left leg position at q^*_1. In the following, we will develop the conditions on q^*_1 and the desired walking pattern $\mathbf{g}_i(l\sin(q_1), q_2, q_3) = \mathbf{0}$ ($i \in \{L, R\}$) such that $\boldsymbol{\Delta}_{L\to R}(\tau^-_K, \mathbf{0}) = \mathbf{0}$ in condition (C1) is satisfied for any $K \in \{1, 3, 5,\ldots\}$.

From Eq. (7), the desired support-leg trajectory $q_{1d}(t)$ will increase monotonically within the Kth step if $s_d(t)$ is planned as feasible and monotonically increasing. Then, the Kth desired landing moment $t = \tau^-_K$, if exists, can be uniquely determined from the equation $q_{1d}(\tau^-_K) = q^*_1$.

Assuming $\mathbf{x}(\tau^-_K) = \mathbf{0}$, one has

$$\mathbf{q}(\tau^-_K) = \mathbf{H}_{qL}(q^*_1) \quad \text{and} \quad \dot{\mathbf{q}}(\tau^-_K) = \mathbf{H}_{\dot{q}L}(q^*_1)\dot{q}_{1d}(\tau^-_K) \tag{48}$$

where

$$\mathbf{H}_{qL}(q_1) := \begin{bmatrix} q_1 \\ \tilde{\phi}_{1L}(q_1) \\ \tilde{\phi}_{2L}(q_1) \end{bmatrix} \quad \text{and} \quad \mathbf{H}_{\dot{q}L}(q_1) := \begin{bmatrix} 1 \\ \dfrac{d\tilde{\phi}_{1L}(q_1)}{dq_1} \\ \dfrac{d\tilde{\phi}_{2L}(q_1)}{dq_1} \end{bmatrix} \tag{49}$$

Then, at $t = \tau^+_K$, one can obtain the following equations from Eq. (5)

$$\begin{aligned} &\mathbf{q}(\tau^+_K) = \mathbf{q}(\tau^-_K) = \mathbf{H}_{qL}(q^*_1), \\ &\dot{\mathbf{q}}(\tau^+_K) = \mathbf{I}_L(\mathbf{q}(\tau^-_K))\dot{\mathbf{q}}(\tau^-_K) = \tilde{\mathbf{I}}_L(q^*_1)\mathbf{H}_{\dot{q}L}(q^*_1)\dot{q}_{1d}(\tau^-_K) \end{aligned} \tag{50}$$

where $\tilde{\mathbf{I}}_L(q^*_1) := \mathbf{I}_L(\mathbf{H}_{qL}(q^*_1)) = \mathbf{I}_L(\mathbf{q}(\tau^-_K))$.

Assuming $\mathbf{x}(\tau^+_K) = \mathbf{0}$, one has

$$\mathbf{q}(\tau^+_K) = \mathbf{H}_{qR}(q_{2d}(\tau^+_K)) \quad \text{and} \quad \dot{\mathbf{q}}(\tau^+_K) = \mathbf{H}_{\dot{q}R}(q_{2d}(\tau^+_K))\dot{q}_{2d}(\tau^+_K) \tag{51}$$

where

$$\mathbf{H}_{qR}(q_2) := \begin{bmatrix} \tilde{\phi}_{1R}(q_2) \\ q_2 \\ \tilde{\phi}_{2R}(q_2) \end{bmatrix} \quad \text{and} \quad \mathbf{H}_{\dot{q}R}(q_2) := \begin{bmatrix} \dfrac{d\tilde{\phi}_{1R}(q_2)}{dq_2} \\ 1 \\ \dfrac{d\tilde{\phi}_{2R}(q_2)}{dq_2} \end{bmatrix} \tag{52}$$

Because $s_d(t)$ is continuously differentiable for $t>0$, one has

$$s_d(\tau^+_K) = s_d(\tau^-_K) \quad \text{and} \quad \dot{s}_d(\tau^+_K) = \dot{s}_d(\tau^-_K) \tag{53}$$

Also, $s(t)$ is continuous for $t>0$. Then, one obtains

$$q_{2d}(\tau^+_K) = \tilde{\phi}_{1L}(q^*_1) \tag{54}$$

and

$$\dot{q}_{2d}(\tau^+_K) = \frac{\cos(q^*_1)}{\cos\left(\tilde{\phi}_{1L}(q^*_1)\right)}\dot{q}_{1d}(\tau^-_K) := \gamma_L(q^*_1)\dot{q}_{1d}(\tau^-_K) \tag{55}$$

Therefore, if $\tilde{\phi}_{ji}$ ($i \in \{L, R\}, j \in \{1, 2\}$) can be designed to satisfy

$$\mathbf{H}_{qL}(q^*_1) = \mathbf{H}_{qR}(\tilde{\phi}_{1L}(q^*_1)) \tag{56}$$

and

$$\tilde{\mathbf{I}}_L(q^*_1)\mathbf{H}_{\dot{q}L}(q^*_1) = \mathbf{H}_{\dot{q}R}(\tilde{\phi}_{1L}(q^*_1))\gamma_L(q^*_1) \tag{57}$$

then $\mathbf{x}(\tau^+_K) = \boldsymbol{\Delta}_{L\to R}(\tau^-_K, \mathbf{0}) = \mathbf{0}$ holds for any $K \in \{1, 3, 5,\ldots\}$.

We will now derive conditions to guarantee that $\boldsymbol{\Delta}_{R\to L}(\tau^-_{K+1}, \mathbf{0}) = \mathbf{0}$ in the condition (C1) holds for any $K \in \{1, 3, 5,\ldots\}$. Similarly, suppose that the desired walking pattern $\mathbf{g}_R(l\sin(q_2), q_1, q_3) = \mathbf{0}$ has at least one intersection with the switching surface $S_R(\mathbf{q}, \dot{\mathbf{q}})$ and that one of these intersections has right leg position at q^*_2. If $\tilde{\phi}_{ji}$ ($i \in \{L, R\}, j \in \{1, 2\}$) is designed to satisfy

$$\mathbf{H}_{qR}(q^*_2) = \mathbf{H}_{qL}(\tilde{\phi}_{1R}(q^*_2)) \tag{58}$$

and

$$\tilde{\mathbf{I}}_R(q^*_2)\mathbf{H}_{\dot{q}R}(q^*_2) = \mathbf{H}_{\dot{q}L}(\tilde{\phi}_{1R}(q^*_2))\gamma_R(q^*_2) \tag{59}$$

with $\tilde{\mathbf{I}}_R(q^*_2) := \mathbf{I}_R(\mathbf{H}_{qR}(q^*_2))$ and $\gamma_R(q^*_2) := (\cos(q^*_2)/\cos(\tilde{\phi}_{1R}(q^*_2)))$, then $\boldsymbol{\Delta}_{R\to L}(\tau^-_{K+1}, \mathbf{0}) = \mathbf{0}$ holds for any $K \in \{1, 3, 5,\ldots\}$.

5.2 Walking Pattern Parameterization With Beziér Curves. Similar to the previous study [12], the functions $\tilde{\phi}_{ji}$ ($i \in \{L, R\}, j \in \{1, 2\}$), which define the desired walking pattern, can be parameterized by the Mth-order Beziér curves as

$$\begin{aligned} \tilde{\phi}_{1L}(q_1) &:= \bar{\phi}_{1L}(\lambda_L) = \sum_{p=0}^{M} \alpha_{Lp} \frac{M!}{p!(M-p)!} \lambda_L^p (1-\lambda_L)^{M-p} \\ \tilde{\phi}_{2L}(q_1) &:= \bar{\phi}_{2L}(\lambda_L) = \sum_{p=0}^{M} \beta_{Lp} \frac{M!}{p!(M-p)!} \lambda_L^p (1-\lambda_L)^{M-p} \\ \tilde{\phi}_{1R}(q_2) &:= \bar{\phi}_{1R}(\lambda_R) = \sum_{p=0}^{M} \alpha_{Rp} \frac{M!}{p!(M-p)!} \lambda_R^p (1-\lambda_R)^{M-p} \\ \tilde{\phi}_{2R}(q_2) &:= \bar{\phi}_{2R}(\lambda_R) = \sum_{p=0}^{M} \beta_{Rp} \frac{M!}{p!(M-p)!} \lambda_R^p (1-\lambda_R)^{M-p} \end{aligned} \tag{60}$$

where α_{ip} and β_{ip} ($i \in \{L, R\}$, $p \in \{0, 1,\ldots, M\}$) are unknown parameters to be determined, and the variables $\lambda_L(q_1)$ and $\lambda_R(q_2)$ are defined as

$$\lambda_L(q_1) = \frac{q_1 - q_{10}}{q^*_1 - q_{10}} \quad \text{and} \quad \lambda_R(q_2) = \frac{q_2 - q_{20}}{q^*_2 - q_{20}} \tag{61}$$

where q_{10} and q_{20} are the initial support-leg angles of the left-in-support and the right-in-support phases, respectively, determined by the desired walking pattern and the switching surfaces.

The functions $\bar{\phi}_{ji}(\lambda_i)$ ($i \in \{L, R\}, j \in \{1, 2\}$) have the following properties [12]:

(1) $\bar{\phi}_{1i}(0) = \alpha_{i0}$, $\bar{\phi}_{2i}(0) = \beta_{i0}$;
(2) $\bar{\phi}_{1i}(1) = \alpha_{iM}$, $\bar{\phi}_{2i}(1) = \beta_{iM}$;
(3) $d\bar{\phi}_{1i}/d\lambda_i(0) = M\alpha_{i1} - \alpha_{i0}$, $d\bar{\phi}_{2i}/d\lambda_i(0) = M\beta_{i1} - \beta_{i0}$; and
(4) $d\bar{\phi}_{1i}/d\lambda_i(1) = M\alpha_{iM} - \alpha_{i(M-1)}$, $d\bar{\phi}_{2i}/d\lambda_i(1) = M\beta_{iM} - \beta_{i(M-1)}$.

These properties can be utilized to construct hybrid invariance of the desired motion.

5.3 An Example of Walking Pattern Design With Third-Order Beziér Curves. In this subsection, the procedure of obtaining the unknown parameters α_{ip} and β_{ip} ($i \in \{L, R\}$, $p \in \{0, 1, \ldots, M\}$) of $\bar{\phi}_{ji}$ ($i \in \{L,R\}$, $j \in \{1,2\}$) in Eq. (60) is explained. Suppose $M = 3$. From Eqs. (56)–(61) and the properties of $\bar{\phi}_{ji}$ ($i \in \{L,R\}$, $j \in \{1,2\}$), one has

$$q_1^* = \alpha_{R0}, \quad q_2^* = \alpha_{L0}, \quad q_{10} = \alpha_{R3}, \quad q_{20} = \alpha_{L3} \tag{62}$$

$$\lambda_L(q_1) = \frac{q_1 - \alpha_{R3}}{\alpha_{R0} - \alpha_{R3}}, \quad \lambda_R(q_2) = \frac{q_2 - \alpha_{L3}}{\alpha_{L0} - \alpha_{L3}} \tag{63}$$

$$\beta_{L3} = \beta_{R0}, \quad \beta_{L0} = \beta_{R3} \tag{64}$$

$$\gamma_L(\alpha_{R0}) \begin{bmatrix} \dfrac{3\alpha_{R1} - \alpha_{R0}}{\alpha_{L0} - \alpha_{L3}} \\ 1 \\ \dfrac{3\beta_{R1} - \beta_{R0}}{\alpha_{L0} - \alpha_{L3}} \end{bmatrix} = \tilde{\mathbf{I}}_L(\alpha_{R0}) \begin{bmatrix} 1 \\ \dfrac{3\alpha_{L3} - \alpha_{L2}}{\alpha_{R0} - \alpha_{R3}} \\ \dfrac{3\beta_{L3} - \beta_{L2}}{\alpha_{R0} - \alpha_{R3}} \end{bmatrix} \tag{65}$$

$$\gamma_R(\alpha_{L0}) \begin{bmatrix} 1 \\ \dfrac{3\alpha_{L1} - \alpha_{L0}}{\alpha_{R0} - \alpha_{R3}} \\ \dfrac{3\beta_{L1} - \beta_{L0}}{\alpha_{R0} - \alpha_{R3}} \end{bmatrix} = \tilde{\mathbf{I}}_R(\alpha_{L0}) \begin{bmatrix} \dfrac{3\alpha_{R3} - \alpha_{R2}}{\alpha_{L0} - \alpha_{L3}} \\ 1 \\ \dfrac{3\beta_{R3} - \beta_{R2}}{\alpha_{L0} - \alpha_{L3}} \end{bmatrix} \tag{66}$$

The function $\tilde{\phi}_{ji}$ ($i \in \{L,R\}$, $j \in \{1,2\}$) should also satisfy the following switching conditions obtained from Eq. (3) (forward walking direction is assumed):

$$\begin{aligned} & l\cos(\alpha_{R0}) - l\cos(\alpha_{L3}) = 0 \\ & -l\sin(\alpha_{R0}) + l\sin(\alpha_{L3})\frac{3\alpha_{L3} - \alpha_{L2}}{\alpha_{R0} - \alpha_{R3}} < 0 \\ & l\cos(\alpha_{L0}) - l\cos(\alpha_{R3}) = 0 \\ & -l\sin(\alpha_{L0}) + l\sin(\alpha_{R3})\frac{3\alpha_{R3} - \alpha_{R2}}{\alpha_{L0} - \alpha_{L3}} < 0 \end{aligned} \tag{67}$$

There are 16 unknown parameters of the four third-order Beziér curves, and there are ten equations and two inequality constraints in Eqs. (64)–(67). Therefore, the function $\tilde{\phi}_{ji}$ ($i \in \{L,R\}$, $j \in \{1,2\}$) can be determined through numerical search in order to satisfy the first condition (C1).

6 Simulation Results

In this section, a fully actuated planar biped with three revolute joints is simulated to show the validity of the proposed walking strategy. We first compare our proposed walking strategy with previous studies to show that we can achieve exponential position tracking in Cartesian space but the previous study can only achieve exponential velocity tracking. Then, a symmetric walking pattern is simulated with two different desired global position trajectories $s_d(t)$–one with a constant walking speed and the other with a time-varying walking speed—to show the versatility of the proposed walking strategy. The simulation results also show that the desired gait respects the reset map regardless of the choice of $s_d(t)$ when the desired walking pattern is designed as introduced in Sec. 5. Furthermore, exponential tracking of an asymmetric walking pattern is illustrated through simulations. Finally, effects of the continuous-phase convergence rate on the closed-loop stability

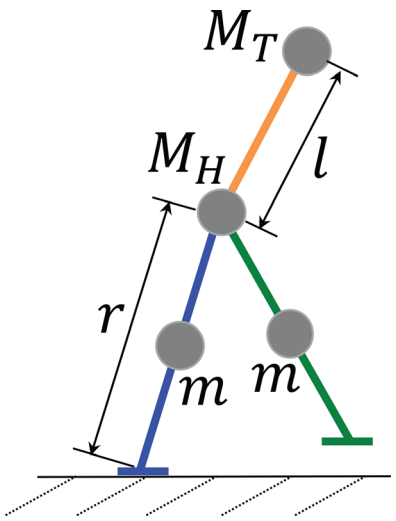

Fig. 3 A planar biped with lumped masses, massless thin feet, and identical legs. ($m = 10$ kg, $M_H = 5$ kg, $M_T = 5$ kg, and $l = (r/2) = 0.5$ m.)

are analyzed through simulations, which validates the stability conditions in Sec. 4.

The simulated biped model is shown in Fig. 3. The definitions of l and r are illustrated in Fig. 3, and the masses m, M_H, and M_T are lumped at the center of each link.

With the walking pattern design proposed in Sec. 5, a symmetric walking pattern and an asymmetric walking pattern are generated, which will be utilized in the following simulations. The obtained swing-leg patterns are shown in Fig. 4 (the trunk patterns are omitted).

6.1 Comparison With Previous Work on Orbital Stabilization. In the previous work on orbital stabilization [11], the bipedal gait is characterized by the support and the swing legs. Thus, only a symmetric walking pattern can be exponentially tracked. Besides walking pattern tracking, another control objective of the previous work is velocity tracking in Cartesian space.

In order to compare our proposed walking strategy with the previous orbital stabilization [11], the desired walking pattern is chosen as the symmetric walking pattern in Fig. 4(*a*). The desired global position trajectory $s_d(t)$ is defined as monotonically increasing with a constant speed. Because the previous walking strategy focuses on velocity tracking in Cartesian space, its desired global motion is defined as $\dot{s}_d(t)$.

The simulation results corresponding to the previous work are shown in Fig. 5. From Fig. 5, it is clear to see that exponential tracking of the desired symmetric walking pattern is achieved. However, there is always a nonzero steady-state tracking error of the desired global position trajectory $s_d(t)$, although the desired global velocity trajectory $\dot{s}_d(t)$ can be exponentially tracked.

In contrast, with our proposed walking strategy, we can realize exponential walking pattern tracking and exponential global position tracking, as shown in Fig. 6.

This comparison clearly illustrates that our proposed walking strategy can greatly improve walking versatility as compared with the previous work on orbital stabilization.

6.2 Exponential Tracking of Different Global Position Trajectories. In this subsection, we will show two sets of simulated bipedal walking with the same desired symmetric walking pattern (see Fig. 4(*a*)) but different desired hip trajectories $s_d(t)$. Without loss of generality, the control gains are chosen the same for both cases: $\mathbf{K}_{PL} = \mathbf{K}_{PR} = \text{diag}[28, 28, 28]$ and $\mathbf{K}_{DL} = \mathbf{K}_{DR} = \text{diag}[11, 11, 11]$. These control gains are chosen such that the matrices $\mathbf{A}_L$ and $\mathbf{A}_R$ in Eq. (20) are both Hurwitz and that the

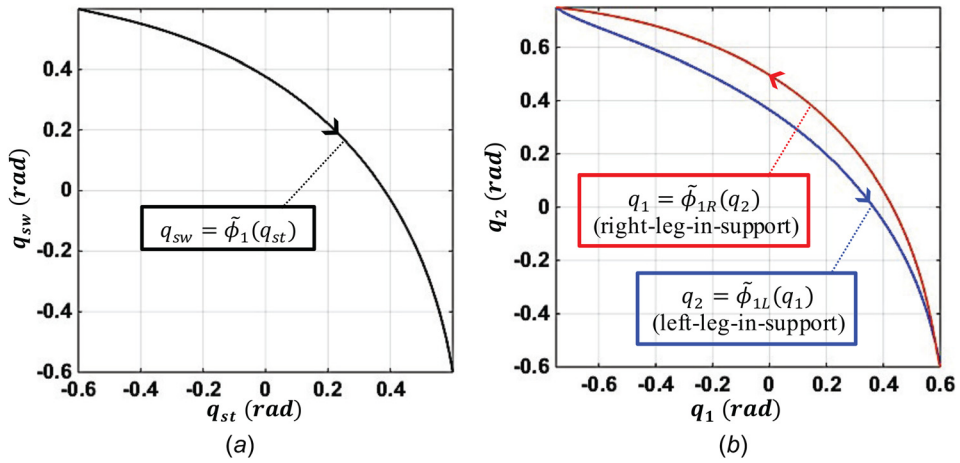

Fig. 4 Desired walking patterns of swing-leg angle q_{sw} with respect to support-leg angle q_{st}: (*a*) symmetric and (*b*) asymmetric

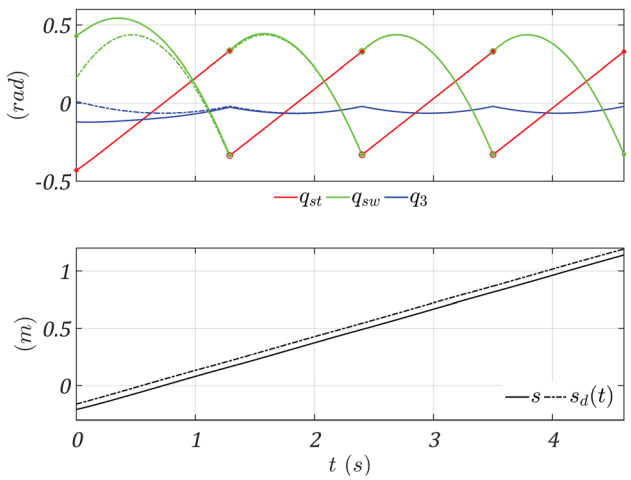

Fig. 5 Simulation results of previous work based on orbital stabilization and support-swing gait characterization. Green (blue) dashed: desired swing-leg (trunk) trajectory determined by the desired walking pattern.

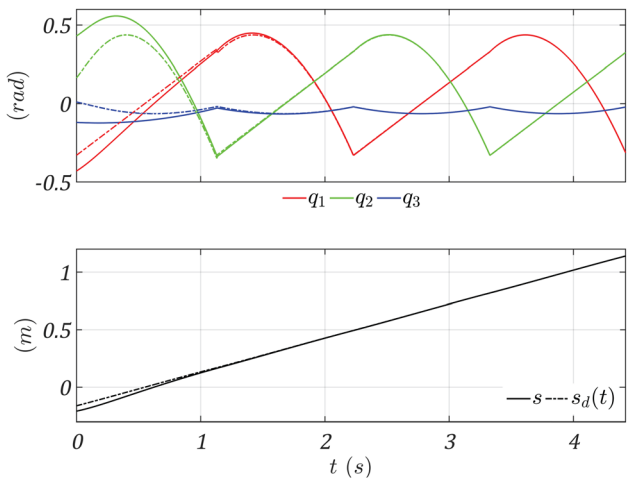

Fig. 6 Simulation results of proposed walking strategy under the left-right gait characterization. Dashed lines: desired joint trajectories generated by $g_i(\bar{s}, q_{sw}, q_3) = 0\,(i \in \{L, R\})$ and $s_d(t)$.

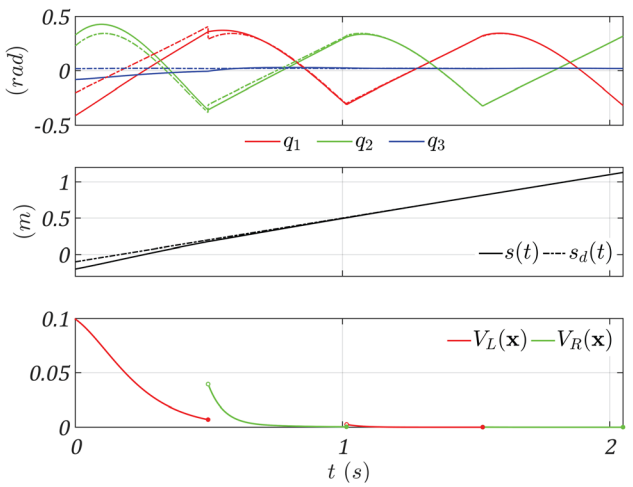

Fig. 7 Symmetric walking with $s_d(t) = 0.6t - 0.1$ m, $K_{Pi} = \text{diag}$ [28, 28, 28], and $K_{Di} = \text{diag}$[11, 11, 11]. Dashed lines: desired joint trajectories generated by $g_i(\bar{s}, q_{sw}, q_3) = 0\,(i \in \{L, R\})$ and $s_d(t)$.

conditions in Eqs. (46) and (47) are met under relatively large initial tracking errors. The two sets of bipedal walking share the same initial conditions

$$\begin{aligned} s(0) - s_d(0) &= -0.1(\text{m}),\ \dot{s}(0) - \dot{s}_d(0) = 0.1(\text{m/s}) \\ q_2(0) - \tilde{\phi}_{1L}(q_1(0)) &= 0.1(\text{rad}) \\ q_3(0) - \tilde{\phi}_{2L}(q_1(0)) &= -0.1(\text{rad}) \\ \dot{q}_2(0) - \frac{d\tilde{\phi}_{1L}}{dq_1}(q_1(0))\dot{q}_1(0) &= -0.1(\text{rad/s}) \\ \dot{q}_3(0) - \frac{d\tilde{\phi}_{2L}}{dq_1}(q_1(0))\dot{q}_1(0) &= 0.1(\text{rad/s}) \end{aligned} \tag{68}$$

Due to the identical control gains, one has $\mathbf{A} = \mathbf{A}_L = \mathbf{A}_R$. Then, without loss of generality, the Lyapunov functions during the left-in-support and the right-in-support phases are chosen the same

$$V_L(\mathbf{x}) = V_R(\mathbf{x}) = \mathbf{x}^{\mathrm{T}}\mathbf{W}\mathbf{x} \tag{69}$$

where $\mathbf{W}$ is the solution of the Lyapunov equation $\mathbf{A}\mathbf{W} + \mathbf{W}\mathbf{A}^{\mathrm{T}} + \mathbf{Q} = \mathbf{0}$ with $\mathbf{Q} = \mathbf{I}_{6\times 6}$ [30].

Figure 7 shows the results with $s_d(t) = 0.6t - 0.1(\text{m})$, and Fig. 8 corresponds to $s_d(t) = 2.3e^{-0.3(t+0.5)} + 0.6t - 2.1(\text{m})$. From the plots, we can see that exponential tracking of the desired hip

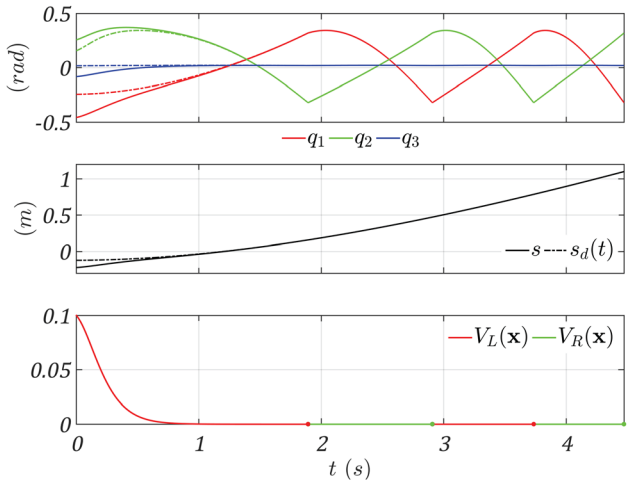

Fig. 8 Symmetric walking with $s_d(t) = 2.3e^{-0.3(t+0.5)} + 0.6t - 2.1$(m), $K_{Pi} = \text{diag}[28, 28, 28]$, and $K_{Di} = \text{diag}[11, 11, 11]$. Dashed lines: desired joint trajectories generated by $g_i(\bar{s}, q_{sw}, q_3) = 0$ ($i \in \{L, R\}$) and $s_d(t)$.

trajectory $s_d(t)$ with either a constant or a time-varying walking speed is achieved under the same desired walking pattern. It shows that a walking pattern generated through the proposed gait design method in Sec. 5 can be automatically incorporated with an arbitrary hip trajectory $s_d(t)$ that is differentiable and monotonically increasing. Note that the Lyapunov function plot in Fig. 7 shows a relatively large jump at the first impact at $t = 0.5$ s while the one in Fig. 8 shows no significant jump at the first landing impact at $t = 2$ s. Because the desired global position trajectory in Fig. 8 has a much lower velocity in the first few seconds than that in Fig. 7, the duration of the first step is much longer in Fig. 8, which results in the much smaller trajectory tracking error right before the first impact and the much smaller jump of the Lyapunov function right after the first impact in Fig. 8.

6.3 Stable Asymmetric Walking. As stated earlier, the left-right gait characterization enables planning and tracking of an asymmetric walking pattern, which is illustrated with simulation results in this subsection. Figure 9 shows simulated bipedal walking with the initial conditions in Eq. (68), the desired asymmetric walking pattern in Fig. 4(*b*), and the desired global position trajectory $s_d(t) = 0.6t - 0.1$(m). The control parameters are chosen as

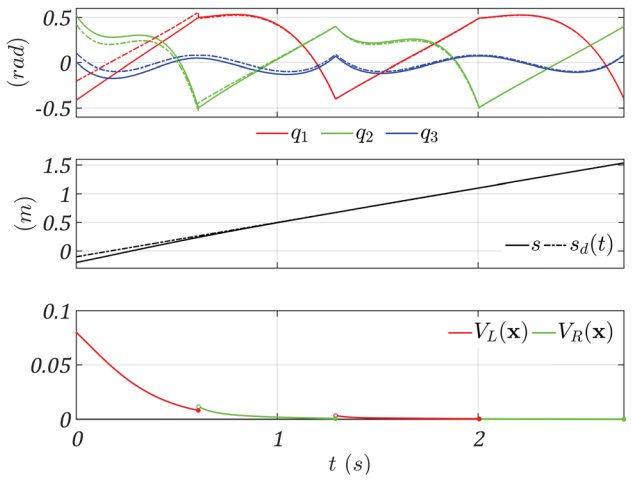

Fig. 9 Asymmetric walking with $s_d(t) = 0.6t - 0.1$ m, $K_{Pi} = \text{diag}[12, 12, 12]$, and $K_{Di} = \text{diag}[7, 7, 7]$. Dashed lines: desired joint trajectories generated by $g_i(\bar{s}, q_{sw}, q_3) = 0$ ($i \in \{L, R\}$) and $s_d(t)$.

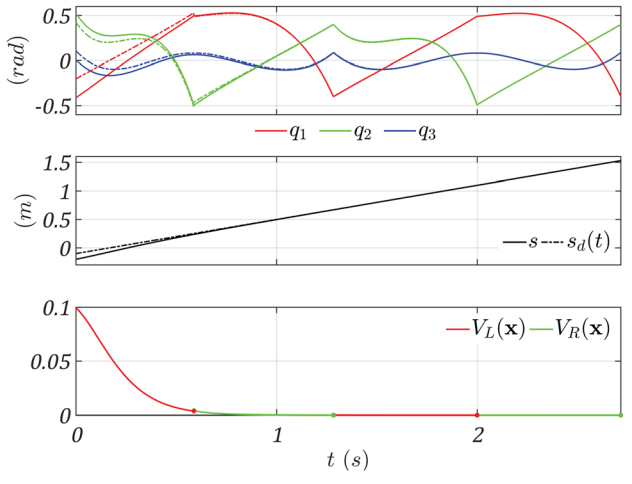

Fig. 10 Asymmetric walking with $s_d(t) = 0.6t - 0.1$ m, $K_{PL} = K_{PR} = \text{diag}[28, 28, 28]$, and $K_{DL} = K_{DR} = \text{diag}[11, 11, 11]$. Dashed lines: desired joint trajectories generated by $g_i(\bar{s}, q_{sw}, q_3) = 0$ ($i \in \{L, R\}$) and $s_d(t)$.

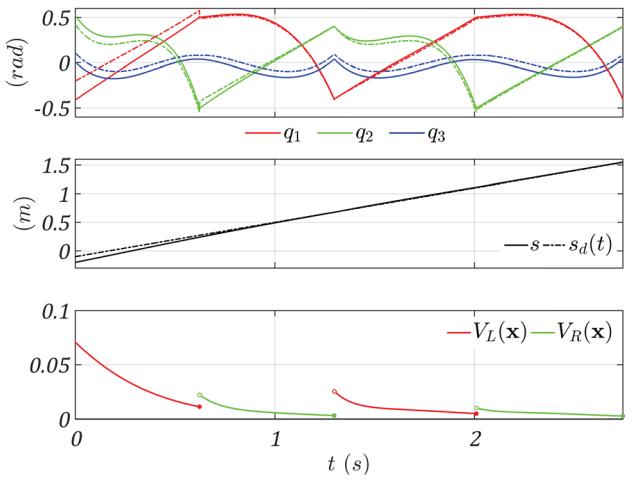

Fig. 11 Asymmetric walking with $s_d(t) = 0.6t - 0.1$ m, $K_{Pi} = \text{diag}[6, 6, 6]$, and $K_{Di} = \text{diag}[5, 5, 5]$. Dashed lines: desired joint trajectories generated by $g_i(\bar{s}, q_{sw}, q_3) = 0$ ($i \in \{L, R\}$) and $s_d(t)$.

$\mathbf{K}_{PL} = \mathbf{K}_{PR} = \text{diag}[12, 12, 12]$ and $\mathbf{K}_{DL} = \mathbf{K}_{DR} = \text{diag}[7, 7, 7]$, and the Lyapunov functions are defined as Eq. (69).

As shown in Fig. 9, the desired asymmetric walking pattern as well as the desired global position trajectory is exponentially tracked, which validates the high versatility of our proposed walking strategy.

6.4 Effects of Continuous-Phase Convergence Rate on Closed-Loop Stability. Theorem 2 introduced in Sec. 4 indicates that the continuous-phase convergence rate determined by the PD gains should be sufficiently fast to guarantee the stability of the closed-loop hybrid dynamical system in Eq. (24). In this subsection, two sets of simulated bipedal walking (see Figs. 10 and 11) are presented under different PD gains. They share the same initial conditions, desired walking pattern, desired hip trajectory, and Lyapunov function definitions as in Fig. 9. However, the PD gains corresponding to Fig. 10 are larger than those in Fig. 9, and the PD gains corresponding to Fig. 11 are less than those in Fig. 9. Accordingly, it can be seen from Figs. 9–11 that the actual motion converges to the desired motion faster in Fig. 10 but slower in Fig. 11 as compared with Fig. 9. Therefore, this comparison

validates Theorem 2 and shows that a higher convergence rate during the continuous phases results in faster closed-loop convergence.

7 Conclusion

In this paper, provably stable, fully actuated, planar bipedal robotic walking has been achieved with improved versatility as compared with previous studies. In order to define both symmetric and asymmetric walking patterns, the left and the right legs were used to characterize a bipedal gait. Under the left–right gait characterization, the full-order hybrid walking dynamics were modeled. With the output function designed as the global position tracking error and the walking pattern tracking error, an input–output linearizing controller was then synthesized to exponentially drive the output function to zero. Closed-loop stability conditions were analyzed based on the construction of multiple Lyapunov functions, which essentially requires that the continuous-phase convergence rate of the output function should be sufficiently fast in order to overcome the possible divergence caused by landing impacts. A new method of walking pattern design was proposed, which guarantees that the low-level planning of the desired walking pattern can be decoupled from the high-level planning of the desired global motion. Provable exponential stabilization and high versatility of the proposed walking strategy were validated with simulated bipedal walking.

Acknowledgment

Any opinion, findings, and conclusions or recommendations expressed in this material are those of the authors and do not necessarily reflect the views of the National Science Foundation.

Funding Data

- Division of Information and Intelligent Systems, National Science Foundation (Grant No. IIS-0916807).

References

[1] Vukobratović, M., and Stepenenko, J., 1972, "On the Stability of Anthropomorphic Systems," Math. Biosci., **15**(1), pp. 1–37.

[2] Kajita, S., Kanehiro, F., Kaneko, K., Fujiwara, K., Harada, K., Yokoi, K., and Hirukawa, H., 2003, "Biped Walking Pattern Generation by Using Preview Control of Zero-Moment Point," IEEE International Conference on Robotics and Automation (ICRA), Taipei, Taiwan, Sept. 14–19, pp. 1620–1626.

[3] Aubin, J. P., 2009, *Viability Theory*, Springer, Berlin.

[4] Wieber, P., 2002, "On the Stability of Walking Systems," International Workshop on Humanoid and Human Friendly Robotics, Tsukuba, Japan, Dec. 11–12, pp. 53–59.

[5] Pratt, J. E., Carff, J., Drakunov, S., and Goswami, A., 2006, "Capture Point: A Step Toward Humanoid Push Recovery," IEEE-RAS International Conference on Humanoid Robots (ICHR), Genova, Italy, Dec. 4–6, pp. 200–207.

[6] Pratt, J., and Tedrake, R., 2006, "Velocity-Based Stability Margins for Fast Bipedal Walking," *Fast Motions in Biomechanics and Robotics*, Springer, Berlin, pp. 299–324.

[7] Koolen, T., De Boer, T., Rebula, J., Goswami, A., and Pratt, J., 2012, "Capturability-Based Analysis and Control of Legged Locomotion—Part 1: Theory and Application to Three Simple Gait Models," Int. J. Rob. Res., **31**(9), pp. 1094–1113.

[8] Pratt, J., Koolen, T., De Boer, T., Rebula, J., Cotton, S., Carff, J., Johnson, M., and Neuhaus, P., 2012, "Capturability-Based Analysis and Control of Legged Locomotion—Part 2: Application to M2V2, a Lower-Body Humanoid," Int. J. Rob. Res., **31**(10), pp. 1117–1133.

[9] Grizzle, J., Abba, G., and Plestan, P., 2001, "Asymptotically Stable Walking for Biped Robots: Analysis Via Systems With Impulse Effects," IEEE Trans. Autom. Control, **46**(1), pp. 51–64.

[10] Grizzle, J. W., Chevallereau, C., Sinnet, R. W., and Ames, A. D., 2014, "Models, Feedback Control, and Open Problems of 3D Bipedal Robotic Walking," Automatica, **50**(8), pp. 1955–1988.

[11] Ames, A. D., Cousineau, E. A., and Powell, M. J., 2012, "Dynamically Stable Bipedal Robotic Walking With NAO Via Human-Inspired Hybrid Zero Dynamics," International Conference on Hybrid Systems: Computation and Control (HSCC), Beijing, China, Apr. 17–19, pp. 135–144.

[12] Westervelt, E. R., Grizzle, J. W., and Koditschek, D. E., 2003, "Hybrid Zero Dynamics of Planar Biped Walkers," IEEE Trans. Autom. Control, **48**(1), pp. 42–56.

[13] Morris, B., and Grizzle, J. W., 2009, "Hybrid Invariant Manifolds in Systems With Impulse Effects With Application to Periodic Locomotion in Bipedal Robots," IEEE Trans. Autom. Control, **54**(8), pp. 1751–1764.

[14] Morris, B., and Grizzle, J. W., 2005, "A Restricted Poincaré Map for Determining Exponentially Stable Periodic Orbits in Systems With Impulse Effects: Application to Bipedal Robots," IEEE International Conference on Decision and Control (CDC), Seville, Spain, Dec. 10–15, pp. 4199–4206.

[15] Griffin, B., and Grizzle, J., 2015, "Walking Gait Optimization for Accommodation of Unknown Terrain Height Variations," American Control Conference (ACC), Chicago, IL, July 1–3, pp. 4810–4817.

[16] Buss, B. G., Ramezani, A., Hamed, K. A., Griffin, B., Galloway, K. S., and Grizzle, J. W., 2014, "Preliminary Walking Experiments With Underactuated 3D Bipedal Robot MARLO," IEEE International Conference on Robots and Systems (IROS), Chicago, IL, Sept. 14–18, pp. 2529–2536.

[17] Da, X., Harib, O., Hartley, R., Griffin, B., and Grizzle, J. W., 2016, "From 2D Design of Underactuated Bipedal Gaits to 3D Implementation: Walking With Speed Tracking," IEEE Access, **4**, pp. 3469–3478.

[18] Shiriaev, A., Perram, J. W., and Canudas-de Wit, C., 2005, "Constructive Tool for Orbital Stabilization of Underactuated Nonlinear Systems: Virtual Constraints Approach," IEEE Trans. Autom. Control, **50**(8), pp. 1164–1176.

[19] Shiriaev, A. S., Freidovich, L. B., and Manchester, I. R., 2008, "Can We Make a Robot Ballerina Perform a Pirouette? Orbital Stabilization of Periodic Motions of Underactuated Mechanical Systems," Annu. Rev. Control, **32**(2), pp. 200–211.

[20] Manchester, I. R., Mettin, U., Iida, F., and Tedrake, R., 2011, "Stable Dynamic Walking Over Uneven Terrain," Int. J. Rob. Res., **30**(3), pp. 265–279.

[21] Ames, A. D., Galloway, K., Sreenath, K., and Grizzle, J. W., 2014, "Rapidly Exponentially Stabilizing Control Lyapunov Functions and Hybrid Zero Dynamics," IEEE Trans. Autom. Control, **59**(4), pp. 876–891.

[22] Ames, A. D., 2014, "Human-Inspired Control of Bipedal Walking Robots," IEEE Trans. Autom. Control, **59**(5), pp. 1115–1130.

[23] Hamed, K. A., and Grizzle, J. W., 2014, "Event-Based Stabilization of Periodic Orbits for Underactuated 3-D Bipedal Robots With Left-Right Symmetry," IEEE Trans. Rob., **30**(2), pp. 365–381.

[24] Branicky, M. S., 1998, "Multiple Lyapunov Functions and Other Analysis Tools for Switched and Hybrid Systems," IEEE Trans. Autom. Control, **43**(4), pp. 475–482.

[25] Gu, Y., Yao, B., and Lee, C. S. G., 2016, "Bipedal Gait Recharacterization and Walking Encoding Generalization for Stable Dynamic Walking," IEEE International Conference on Robotics and Automation (ICRA), Stockholm, Sweden, May 16–21, pp. 1788–1793.

[26] Ramezani, A., Hurst, J. W., Hamed, K. A., and Grizzle, J. W., 2013, "Performance Analysis and Feedback Control of ATRIAS, a Three-Dimensional Bipedal Robot," ASME J. Dyn. Syst. Meas. Control, **136**(2), p. 021012.

[27] Hamed, K. A., Buss, B. G., and Grizzle, J. W., 2016, "Exponentially Stabilizing Continuous-Time Controllers for Periodic Orbits of Hybrid Systems: Application to Bipedal Locomotion With Ground Height Variations," Int. J. Rob. Res., **35**(8), pp. 977–999.

[28] Grizzle, J. W., Abba, G., and Plestan, F., 1999, "Proving Asymptotic Stability of a Walking Cycle for a Five DOF Biped Robot Model," International Conference on Climbing and Walking Robots, Portsmouth, UK, Sept. 14–15, pp. 4048–4053.

[29] Yao, B., Hu, C., and Wang, Q., 2012, "An Orthogonal Global Task Coordinate Frame for Contouring Control of Biaxial Systems," IEEE Trans. Mechatron., **17**(4), pp. 622–634.

[30] Khalil, H. K., 1996, *Nonlinear Control*, Prentice Hall, Upper Saddle River, NJ.

[31] Bainov, D., and Simeonov, P., 1993, *Impulsive Differential Equations: Periodic Solutions and Applications*, Vol. 66, CRC Press, Boca Raton, FL.